Optimized Stokes polarimeters based on a single twisted nematic liquid-crystal device for the minimization of noise propagation

Alba Peinado,[1,*] Angel Lizana,[1] Josep Vidal,[1,2] Claudio Iemmi,[3] and Juan Campos[1]

[1]Departamento de Física, Universitat Autònoma de Barcelona, Bellatera 08193, Spain

[2]ALBA Synchrotron Light Source Facility, Cerdanyola del Vallès 08290, Spain

[3]Departamento de Física, Facultad de Ciencias Exactas y Naturales, Universidad de Buenos Aires, Buenos Aires 1428, Argentina

*Corresponding author: Alba.Peinado@uab.es

Received 29 April 2011; revised 26 July 2011; accepted 29 July 2011; posted 1 August 2011 (Doc. ID 146799); published 26 September 2011

This work evidences the suitability of applying a single twisted nematic liquid-crystal (TN-LC) device to obtain dynamic polarimeters with high accuracy and repeatability. Different Stokes polarimeter setups based on a TN-LC device are optimized, leading to the minimization of the noise propagated from intensity measurements to the Stokes vector calculations. To this aim, we revise the influence of working out of normal incidence and of performing a double pass of the light beam through the LC device. In addition, because transmissive TN-LC devices act as elliptical retarders, an extra study is performed. It analyzes the influence of projecting the light exiting from the TN-LC device over elliptical states of polarization. Finally, diverse optimized polarimeters are experimentally implemented and validated by measuring different states of partially and fully polarized light. The analysis is conducted both for monochromatic (He–Ne laser) and LED light sources, proving the potential of polarimeters based on a single TN-LC device. © 2011 Optical Society of America

OCIS codes: 120.5410, 120.2130, 230.3720.

1. Introduction

Polarimetric information is useful in a large number of applications [1–4]. Recently, many works have proposed polarimeters based on liquid-crystal displays (LCDs) [5–12], which present some operational benefits with respect to mechanical polarimeters. Some studies have designed complete polarimeters based on parallel aligned liquid-crystal (LC) devices [5,7], showing that for the experimental implementation of such devices, the use of two parallel aligned LCD elements is required as a minimum [5]. In addition, polarimeters based on the ferroelectric liquid crystal (FLC) are present in the literature. For example, in Refs. [8,9], complete Stokes and Mueller polarimeters based on two FLCs are analyzed, respectively, whereas in Ref. [10], an imaging linear polarimeter based on a single FLC is studied. Other authors have proposed polarimeters based on twisted nematic liquid crystals (TN-LCs), as for instance in Ref. [11] where a polarimeter based on two TN-LC devices, in which only the purely unswitched and fully switched states are applied, is provided.

Taking advantage that TN-LC devices enable both introducing a retardance and rotating the polarization ellipse orientation, a complete Stokes polarimeter based on a single LC device is achieved in Ref. [12]. Nevertheless, such a polarimeter setup is strongly affected by experimental noise, becoming a significant drawback in the application of polarimeters based on a single TN-LC device. These polarimeters are restricted to a certain set of projection

0003-6935/11/285437-09$15.00/0

states of polarization (SOPs), i.e., the available projection SOPs describe a specific curve into the Poincaré sphere [13]. Because projection SOPs configurations enclosing large volumes into the Poincaré sphere are related to lower error propagation values [5], the restriction of a specific projection SOPs curve limits the efficiency of the polarimeter.

In this paper, we propose to vary different physical parameters and to apply an optimization process in order to achieve diverse polarimeter designs based on a single TN-LC device, leading to projection SOP curves enclosing higher volumes into the Poincaré sphere (i.e., lower noise propagation). First, we analyze the influence of working out of normal incidence on the TN-LC polarimeter performance. Besides, the effect of performing a double pass of the light beam through the LC device is revised as well. Finally, by taking into account the fact that transmissive TN-LC devices act as elliptical retarders, we analyze the effect of including in the polarimeter design a quarter-wave plate (QWP). This allows us to project the light exiting from the TN-LC device over the elliptical SOP.

2. Polarimeter Design

Different complete polarimeter designs are presented in this work, all of them based on a single off-the-shelf monopixel TN-LC device and a linear polarizer (LP). In the first proposed design (now denoted as A), a polarizer and a TN-LC device are set perpendicular to the incident beam [it is sketched in Fig. 1(a)]. In the second design (B), the TN-LC is tilted at an angle of α_2 [see Fig. 1(b)] with the purpose of working out of normal incidence. Next, a third polarimeter setup (C) is conducted by doubling the optical path into the LC device. It is achieved by means of a reflection on a mirror [see Fig. 1(c)].

The Mueller matrices of the TN-LC device for configurations A, B, and C have been calibrated. For the particular case of setup C, we have calibrated the Mueller matrix that takes into account the double pass of the light through the TN-LC device and the reflection on the mirror. These matrices are calibrated as a function of the addressed voltage to the TN-LC device by applying the method developed in Ref. [14]. Afterward, we have simulated the set of possible projection SOPs that can be implemented in the three different setups (A, B, and C) by sending a sequence of voltages from 1 to 5.5 V (i.e., the LC operative range). The projection of the light exiting from the TN-LC device over a linear SOP (i.e., over the polarizer), defines a specific projection SOP curve that is strongly dependent on the polarizer orientation θ. For this reason, we have optimized the angle θ by minimizing the figure-of-merit so-called equally weighted variance (EWV) [5,15]. This quality indicator (QI) expresses the variance propagation from intensity measurements, I, through the characteristic polarimeter matrix, A, to the Stokes vector calculation, S, according to Eq. (1) describing the measurement principle:

$$S = A^{-1}I. \tag{1}$$

The definition of the EWV is given by Eq. (2), where all the singular values different from zero, σj, of the characteristic polarimeter matrix A contribute in the summation:

$$\mathrm{EWV}(A) = \sum_j \frac{1}{\sigma_j^2}. \tag{2}$$

Once the projection SOP curve has been optimized (i.e., the best LP orientation is found), we have searched for the optimum set of four projection SOPs by carrying out a second minimization of the EWV. Note that this is exactly the minimum number of intensity measurements required to implement a complete polarimeter. The results achieved in the optimization process are shown in Table 1 (columns A, B, and C correspond to the three analyzed

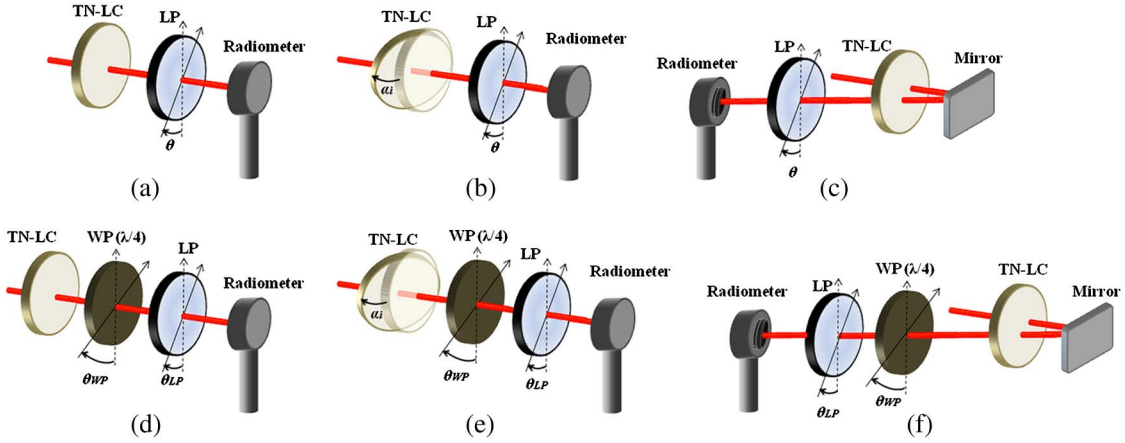

Fig. 1. (Color online) Different Stokes polarimeter setups containing a single TN-LC, an LP, and a radiometer: (a) normal incidence, (b) oblique incidence at αi on the TN-LC, (c) double pass through the TN-LC device by means of a reflection on a mirror, (d) normal incidence and inserting a QWP [WP(λ/4)] between the TN-LC and the polarizer, (e) TN-LC oblique incidence including a QWP, and (f) TN-LC double pass including a QWP.

Table 1. Optimization Results by Minimizing the EWV Indicator Corresponding to Polarimeters A–F (Using Four Projection SOPs)[a]

	A	B	C	D	E	F
LP θ	15°	136°	94°	31°	120°	109°
WP θ	—	—	—	49°	43°	0°
EWV	6.82	4.88	3.70	3.50	3.88	2.78
CN	4.66	3.61	2.69	2.69	3.06	1.98

[a]In the first two rows are the optimum LP orientation and QWP angle. In the last two rows are QI (CN and EWV) values corresponding to the optimized polarimeters.

polarimeters up to now). Although the EWV is the QI employed in the optimization process, we have also calculated another widespread used QI, the condition number [5,7] (CN). The definition of the CN is not unique: in this work it is calculated as the ratio of the maximum over the minimum singular value of the characteristic polarimeter matrix A:

$$\mathrm{CN}(A) = \frac{\sigma_{\max}}{\sigma_{\min}}. \tag{3}$$

Regarding polarimeters A and B, it is noticeable that lower CN and EWV values are obtained for oblique incidence. Thus, an enlargement of the optical path causes a modification of the LC birefringence, which leads to alternative projection SOPs curves. The same idea is present in polarimeter C. In fact, the double pass performed by the light beam into the TN-LC device leads to a significant enlargement of the optical path, achieving lower QI values than in polarimeters A and B.

As stated before, the projection SOPs curve strongly depends on the linear SOP on which the light exiting from the TN-LC device is projected (i.e., the orientation of the LP). As transmissive TN-LC devices act as elliptical retarders [16] (i.e., their eigenvectors are elliptical [17]), we have also conducted a study of the influence on the QIs obtained when light exiting from TN-LC device is projected over elliptical SOPs. To this aim, we have modified the three polarimeter setups A, B, and C by introducing a QWP between the LP and the TN-LC. This leads to the setups sketched in Figs. 1(d)–1(f), henceforth denoted as polarimeters D, E, and F, respectively. Afterward, we have carried out a first optimization process equivalent to that previously described, but in this case, the QWP angle is optimized as well.

Subsequently, a second EWV minimization is conducted with the aim of selecting the four optimal projection SOPs. In the three last columns of Table 1, the QIs corresponding to polarimeters D, E, and F, respectively, are shown. Whereas a significant decrease of the QIs is observed at normal incidence (comparing polarimeters A and D), the improvement at oblique incidence is less relevant (from B to E). This fact can be understood if it is kept in mind that an elliptical retarder can be described as the product of a linear retarder and a rotator of a given angle [16]. In this situation, when the light impinges out of normal incidence, the effective rotator angle may be decreased. In such a case, projecting the SOP exiting from the TN-LC over an elliptical polarization state has less influence in the optimization process. Finally, concerning polarimeter F, a slight improvement of QIs is obtained when comparing with polarimeter C. In this case, the double pass of the light into the TN-LC device may drastically decrease or even cancel the effective rotator [18]. Therefore, the most beneficial contribution of introducing a QWP in the setup is achieved for normal incidence. We want to emphasize that the diverse improvements applied to the polarimeter setups have led to a progressive reduction of the EWV indicator, reaching a minimum value of 2.78 for polarimeter F (and 1.98 of CN). This is an excellent result if one takes into account the fact that the minimum theoretical values that can be achieved for the EWV and CN are 2.5 and $\sqrt{3}$, respectively [5,15]. In this ideal case, the optimized projection SOPs are plotted on the vertices of a regular tetrahedron inscribed into the Poincaré sphere.

In Fig. 2, we represent the optimized projection SOP curve upon the Poincaré sphere corresponding to the different polarimeters (from A to F). In each graph, the 4 optimal projection SOPs (solution of the complete optimization process) are placed at the vertices of an irregular tetrahedron. As said before, a TN-LC-based polarimeter restricts the available projection SOPs, leading to a specific curve upon the Poincaré sphere (see Fig. 2). In general, it is not certain that the TN-LC specific curve includes four projection SOPs forming a regular tetrahedron inscribed into the Poincaré sphere, and so, the polarimetric setup based on a single TN-LC device most probably is not able to implement the best optimized polarimeter [5,15]. However, the applied optimizations have maximized the projection SOPs curves, leading to irregular tetrahedrons whose volumes are similar to that given by the regular tetrahedron [15].

3. Implementation

In this section, we have experimentally implemented the optimized polarimeters. Two different illumination sources have been used. First, the polarimeter was illuminated by using a monochromatic light source. Second, a red LED was used. In both cases, we have calibrated the implemented polarimeters by following the method given in Ref. [5], to reduce the influence of possible small deviations with respect to the theoretical configurations. Then, the implemented polarimeters were tested by measuring three different incident states fully polarized: a linear SOP at 30°, an elliptical SOP, and a right-handed circular SOP.

The measurement process of the six implemented polarimeters is as following: the voltage signal is sent to the TN-LC device, we wait 500 ms to achieve a stationary position of the LC molecules, and then 100 measurements of the intensity are acquired in a rate of 100 Hz. Because each SOP measurement

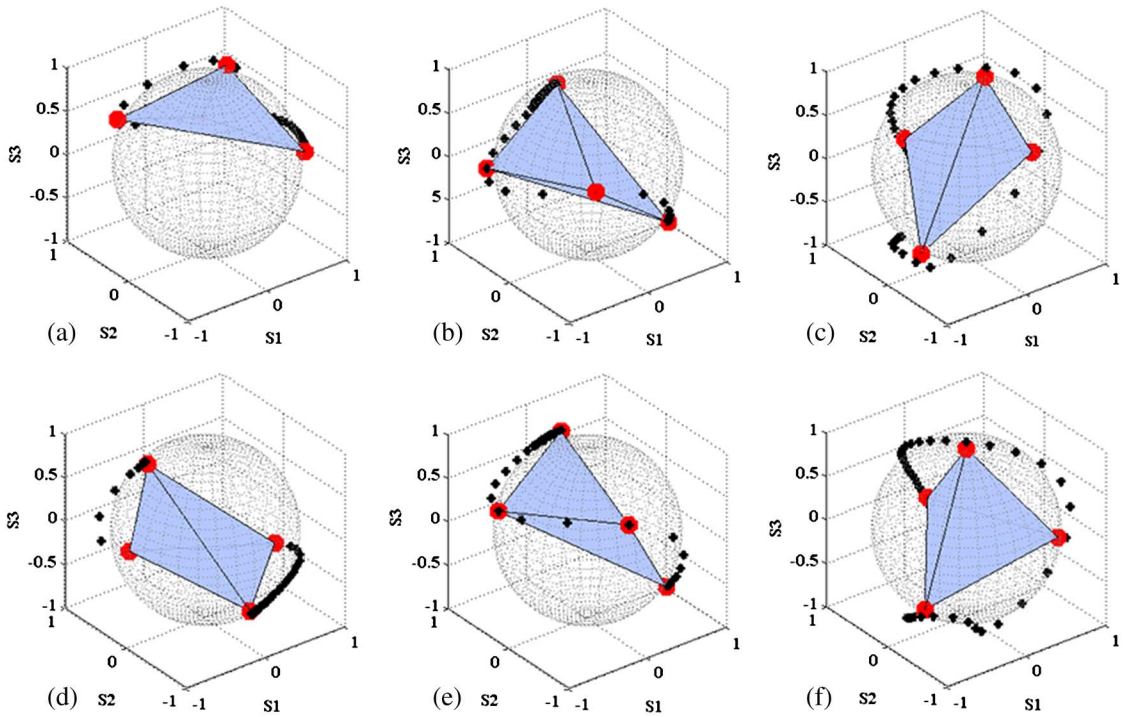

Fig. 2. (Color online) Optimized projection SOPs curve by addressing a sequence of voltages (1–5.5 V) for polarimeters (a) A, (b) B, (c) C, (d) D, (e) E, and (f) F. The vertices of each inscribed irregular tetrahedron are the four optimal projection polarization states achieved as a solution of the EWV minimization process.

performed by the polarimeter needs four intensity measurements, the process is repeated for the four voltages (in other words, using the four projection SOPs). Afterward, the Stokes vector is calculated by using the mean value of the 100 intensity measurements in Eq. (1). That SOP measurement takes around 6 s. Finally, the SOP measurement process is repeated 100 times (it takes approximately 10 min). The experimental data provided in this work correspond to the mean and standard deviation of these 100 measurements of the same SOP. The obtained results are compared with the measurements provided by a commercial polarimeter (Thorlabs, Polarization Analyzer System PAN 5710VIS, S/N: M60217605). Also, 100 measurements for each SOP are performed with the commercial polarimeter, and so the mean and the standard deviation are provided. In addition, we indicate the expected values of the Stokes coefficients to have a reference, although in each measurement the polarization is checked with the commercial polarimeter.

Finally, because the Mueller–Stokes formalism is used, the polarimeter is able to measure partially polarized light. For this reason, we have measured two additional SOPs with a certain degree of polarization (DOP) [13], defined as

$$\mathrm{DOP} = \frac{\sqrt{S_1^2 + S_2^2 + S_3^2}}{S_0}; \qquad 0 \le \mathrm{DOP} \le 1. \quad (4)$$

A. Monochromatic Illumination

The six optimized polarimeters previously described were implemented by using as a light source an He–Ne laser (633 nm). The EWVs of the matrices experimentally calibrated are very close to the theoretical EWV values shown in Table 1. Therefore, in spite of the presence of experimental inaccuracies, the implemented polarimeters were still well optimized when they were illuminated with monochromatic light.

The accuracy of the implemented polarimeters is analyzed in Table 2, where the measures obtained with the implemented polarimeters can be compared with the information provided by the commercial polarimeter. The accuracy is calculated by regarding the difference between the measurements provided by the implemented polarimeter and the commercial polarimeter (reference value). Almost all the measurement differences are in the second decimal, except for a specific case (when polarimeter A measured the S3 parameter in the elliptical SOP, the accuracy got 1 order of magnitude less).

The repeatability of the implemented polarimeters was studied as well. In Fig. 3, the average of the Stokes parameters variances for the different polarimeters is represented. The rhombi in Fig. 3 shows the variance average for polarimeters A, B, and C. When the exiting SOP from TN-LC is projected over a linear SOP, the best result is achieved for the double-pass setup (polarimeter C). The squares in Fig. 3 show the variance averages for polarimeters E, F, and G. When the exiting SOP from the TN-LC is projected over an elliptical SOP, the

Table 2. Stokes Parameters of Three Different SOPs (the Stokes Vectors Are Normalized) Measured by Each Implemented Polarimeter (A, B, C, D, E, and F), when Monochromatic Light Is Employed[a]

	Linear SOP			Elliptical SOP			Circular SOP		
	S1	S2	S3	S1	S2	S3	S1	S2	S3
Expected values	0.5	0.866	0	0	0.866	0.5	0	0	1
A	0.487 ± 0.001	0.883 ± 0.004	0.009 ± 0.002	-0.016 ± 0.001	0.883 ± 0.001	0.194 ± 0.001	-0.016 ± 0.005	0.010 ± 0.003	0.984 ± 0.003
Thorlabs	0.5041 ± 0.0003	0.8635 ± 0.0002	0.0159 ± 0.0004	-0.0063 ± 0.0057	0.8625 ± 0.0012	0.5059 ± 0.0020	0.0247 ± 0.0162	-0.0407 ± 0.0171	0.9986 ± 0.0010
B	0.492 ± 0.002	0.877 ± 0.002	0.019 ± 0.004	-0.027 ± 0.002	0.873 ± 0.001	0.510 ± 0.003	-0.009 ± 0.001	-0.005 ± 0.001	1.005 ± 0.002
Thorlabs	0.4972 ± 0.0005	0.8672 ± 0.0003	0.0265 ± 0.0004	0.0003 ± 0.0007	0.8667 ± 0.0003	0.4988 ± 0.0005	0.0367 ± 0.0023	-0.0515 ± 0.0016	0.9980 ± 0.0001
C	0.503 ± 0.001	0.868 ± 0.001	-0.005 ± 0.001	-0.004 ± 0.002	0.879 ± 0.002	0.515 ± 0.001	0.025 ± 0.002	0.006 ± 0.001	0.999 ± 0.001
Thorlabs	0.5035 ± 0.0007	0.8637 ± 0.0004	-0.0228 ± 0.0007	-0.0214 ± 0.0011	0.8645 ± 0.0003	0.5021 ± 0.0005	0.0479 ± 0.0011	-0.0752 ± 0.0012	0.9960 ± 0.0001
D	0.493 ± 0.001	0.872 ± 0.001	-0.006 ± 0.001	-0.027 ± 0.001	0.874 ± 0.001	0.510 ± 0.001	-0.001 ± 0.001	0.000 ± 0.001	1.004 ± 0.002
Thorlabs	0.5195 ± 0.0003	0.8541 ± 0.0002	-0.0244 ± 0.0004	-0.0345 ± 0.0011	0.8711 ± 0.0022	0.4899 ± 0.0062	0.0166 ± 0.0009	-0.0574 ± 0.0007	0.9982 ± 0.0001
E	0.501 ± 0.001	0.869 ± 0.002	0.000 ± 0.002	-0.032 ± 0.001	0.873 ± 0.001	0.525 ± 0.001	-0.003 ± 0.001	0.000 ± 0.003	1.006 ± 0.003
Thorlabs	0.5081 ± 0.0003	0.8611 ± 0.0002	0.0155 ± 0.0004	-0.0301 ± 0.0005	0.8668 ± 0.0003	0.4978 ± 0.0005	0.0588 ± 0.0012	-0.0441 ± 0.0012	0.9973 ± 0.0001
F	0.481 ± 0.001	0.850 ± 0.001	-0.004 ± 0.001	-0.027 ± 0.002	0.866 ± 0.001	0.508 ± 0.001	-0.004 ± 0.002	-0.005 ± 0.001	1.007 ± 0.001
Thorlabs	0.4937 ± 0.0011	0.8693 ± 0.0006	-0.0235 ± 0.0008	-0.0309 ± 0.0006	0.8681 ± 0.0002	0.4954 ± 0.0004	0.0269 ± 0.0009	-0.0474 ± 0.0003	0.99851 ± 0.00003

[a]SOPs are also measured with the commercial polarimeter (Thorlabs).

Table 3. Normalized Stokes Parameters (Fully Polarized Contribution) and DOP Measurements of Two Different SOPs Partially Polarized by Means of Polarimeter D and the Commercial Polarimeter (Thorlabs), when Monochromatic Light Is Used

		S1	S2	S3	DOP
SOP 1	Polarimeter D	0.669 ± 0.002	0.085 ± 0.004	0.739 ± 0.003	0.742 ± 0.001
	Thorlabs	0.6534 ± 0.0008	0.0812 ± 0.0008	0.7526 ± 0.0006	0.724 ± 0.047
SOP 2	Polarimeter D	-0.249 ± 0.002	-0.038 ± 0.002	0.968 ± 0.002	0.632 ± 0.001
	Thorlabs	-0.2923 ± 0.0012	-0.0053 ± 0.0007	0.9563 ± 0.0004	0.649 ± 0.042

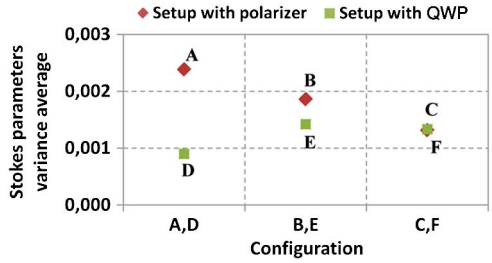

Fig. 3. (Color online) Stokes parameter variance average as a function of different polarimeters, using a linearly polarized SOP (rhombi) or an elliptically polarized SOP (squares) to project over the exiting light from the TN-LC device.

variances are smaller than those obtained for linearly polarized light configurations, this improvement being especially relevant in configuration D. We remark that the EWV is exactly the average of the Stokes parameter variances. Therefore, in Fig. 3 we are representing the experimental EWV obtained from the measurements and so, evidencing experimentally the improvement achieved during the optimization process using the six setups. Note that the tendency shown in Fig. 3 is in agreement with the EWV values of Table 1.

Finally, we have measured two partially polarized states by using polarimeter D, being the polarimeter providing the lowest average variance. The measured SOPs were generated by illuminating a depolarizer (Thorlabs, DPU-25). The light transmitted through this element has a polarization that varies spatially, and because the polarimeter performs an average of a small area, the resulting SOP mean has a certain amount of depolarized light. The DOP measurements obtained are shown in Table 3. Notice that the DOP values between polarimeter D and the commercial one are very close. Moreover, we include the Stokes parameters normalized by $\sqrt{S_1^2 + S_2^2 + S_3^2}$, providing the fully polarized contribution. Again, the experimental results are in agreement. However, small discrepancies between results can be attributed to the difficulty in applying exactly the same measuring area for the two polarimeters. Nevertheless, experimental results evidence the suitability of the polarimeter to measure the polarization of light partially polarized.

B. LED Illumination

Finally, the polarimeter was tested by illuminating with a nonmonochromatic light source. In particular, we have used a red LED (Thorlabs, M625L2), with nominal wavelength 625 nm and a bandwidth of 20 nm. Because birefringence depends on the wavelength, the QWP and the TN-LC device involved in setup D [Fig. 1(d)] may introduce a different retardance to the different wavelengths in the LED spectrum. For this reason, an achromatic QWP was used in the setup. However, a study of the TN-LC achromaticity is important to ensure the same projection SOPs for all the LED wavelengths.

Table 4. Stokes Parameters of Three Different States of Polarization (the Stokes Vectors are Normalized) Measured by Polarimeter D and the Commercial Polarimeter (Thorlabs), when They are Illuminated with an LED Light Source

	Linear SOP			Elliptical SOP			Circular SOP		
	S1	S2	S3	S1	S2	S3	S1	S2	S3
Expected values	0.5	0.866	0	0	0.866	0.5	0	0	1
D	0.494 ± 0.001	0.878 ± 0.001	-0.001 ± 0.001	0.025 ± 0.001	0.839 ± 0.001	-0.4145 ± 0.0004	0.017 ± 0.001	-0.009 ± 0.001	1.002 ± 0.001
Thorlabs	0.4977 ± 0.0003	0.8673 ± 0.0002	-0.0073 ± 0.0001	0.0459 ± 0.0003	0.89404 ± 0.00003	-0.4456 ± 0.0001	-0.0188 ± 0.0001	-0.0344 ± 0.0001	0.99923 ± 0.00001

Table 5. Normalized Stokes Parameters (Fully Polarized Contribution) and DOP Measurements of Two Different SOPs Partially Polarized by Means of Polarimeter D and the Commercial Polarimeter (Thorlabs), when an LED Light Source Is Employed

		S1	S2	S3	DOP
SOP 1	Polarimeter D	-0.019 ± 0.002	-0.114 ± 0.001	0.993 ± 0.002	0.437 ± 0.001
	Thorlabs	-0.0418 ± 0.0002	-0.0647 ± 0.0002	0.99703 ± 0.00001	0.410 ± 0.003
SOP 2	Polarimeter D	-0.044 ± 0.001	0.686 ± 0.001	0.727 ± 0.001	0.5514 ± 0.0004
	Thorlabs	-0.0500 ± 0.0002	0.7120 ± 0.0001	0.7004 ± 0.0001	0.546 ± 0.005

Different optical elements were illuminated with the LED source, and the outcoming SOP was measured with the commercial polarimeter. First, a chromatic waveplate (for 633 nm) was illuminated with linearly polarized light at 45° with respect to the QWP axis. The measured DOP was 0.44. Then, the chromatic retarder was replaced by an achromatic QWP, obtaining a DOP of 0.99. Finally, we have analyzed the effect of illuminating the TN-LC device with linearly polarized light, and the DOP of the exiting SOP was measured for different voltages applied to the TN-LC device. The DOP values were from 0.96 to 1 (i.e., practically fully polarized light). Comparing these data, we have deduced that the TN-LC device is acting as an achromatic element for this bandwidth.

Next, polarimeter D was calibrated, achieving an experimental EWV equal to 3.59. This result is close to the theoretical one (3.50), and it is very similar to that obtained by illumination with monochromatic light (3.57). So, the current polarimeter was also well conditioned for the LED illumination.

Then, we tested the performance when measuring fully polarized states. The SOPs were generated by modifying the polarization of the light beam with a polarizer and an achromatic retarder, to ensure the same incident SOP for all the wavelengths of the LED spectrum and so, generating a fully polarized mean SOP.

In Table 4, we present the measurements of three different fully polarized states. The Stokes parameters obtained with the implemented polarimeter are in accordance to those provided by the commercial polarimeter. The accuracy of the polarimeter, when illuminated with the LED, is of the same order as the one obtained by applying monochromatic light.

Finally, we have completed the study by measuring two partially polarized incoming light beams. The partially polarized SOPs were generated by illuminating a polarizer with the LED light followed by a chromatic QWP. Because the chromatic QWP presents a retardance depending on the wavelength, each wavelength generates a different SOP. Because the polarimeter performs an average measurement, the detected mean SOP had a certain amount of depolarization (i.e., a DOP lower than 1).

In Table 5, two particular cases are provided: SOP 1 and SOP 2. In the first case (SOP 1), the studied SOP was generated by illuminating a polarizer with the LED source followed by a chromatic QWP with its fast axis at 45° of the polarizer transmission axis. In such a case, circular light is obtained for 633 nm (i.e., the QWP operational wavelength), but for the other wavelengths in the LED spectrum, different SOPs are achieved. The measurement obtained with the polarimeter shows a mean SOP almost circularly polarized, accompanied with a significant unpolarized light value (DOP equal to 0.4). The second case (SOP 2) was analogous to the first one, but for a different relative angle between the polarizer transmission axis and the QWP fast axis (i.e., a different mean SOP is obtained).

We want to emphasize that the results given in Tables 4 and 5 prove the potential of the implemented polarimeter, which is able to measure partially or fully polarized light with a nonmonochromatic light source with a small bandwidth (around 20 nm).

4. Simulation of Polarimeters by Changing Some of the TN-LC Cell Features

The monopixel TN-LC cell is extracted from a solar-powered flashing LCD key ring. We emphasize that in this work, the TN-LC characterization by means

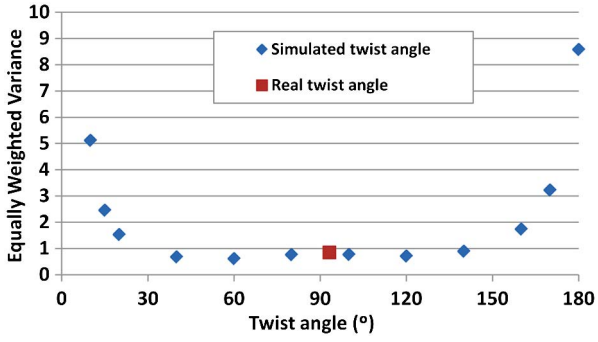

Fig. 4. (Color online) EWV dependence on the twist angle of the TN-LC device. (Actual twist angle value used in the implemented polarimeters in Section 3: 93.2°.)

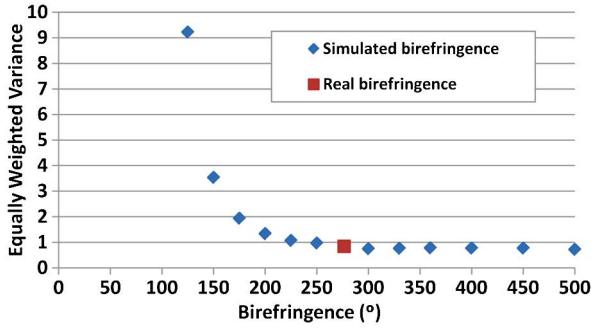

Fig. 5. (Color online) EWV dependence on the maximum birefringence of the TN-LC device. (Actual maximum birefringence value used in the implemented polarimeters in Section 3: 276.5°.)

Table 6. Features of the TN-LC Device Employed in the Polarimeter Setups

Twist Angle (°)	Maximum Birefringence for 633 nm (°)	Orientation of the Molecular Director at the Input Face (°)
93.24	276.51	48.01

of Mueller matrices as a function of the voltage is enough to optimize and implement the presented polarimeters. Nevertheless, in order to have extra information about the physical properties of the LCD device used, we have conducted an additional experimental characterization by following the method explained in Ref. [19]. In Table 6, we show the calibrated parameters of our particular TN-LC cell: total twist angle, the maximum birefringence when illuminating with 633 nm and the orientation of the molecular director at the input face.

Afterward, we simulated the simplest TN-LC polarimeter setup, corresponding to Fig. 1(a), by applying a mathematical model of the TN-LC cell developed in Ref. [20]. In particular, two studies have been conducted in order to analyze the influence of the TN-LC birefringence and the twist angle on the polarimeter optimization. Several projection SOP curves are simulated, each one is composed by the same number of projection SOPs (46) and changing one of the TN-LC parameters (twist angle or maximum birefringence). The parameter unchanged keeps the calibrated value shown in Table 6.

First, the influence of the twist angle is discussed. Simulations of TN-LC device with a different twist angle, from 0° to 180°, are analyzed. The EWV of the simulated projection SOP curves are plotted in the graph of Fig. 4. Notice that TN-LC devices with a twist angle from 40° to 140° give low EWV values of the same order. In addition, the use of a supertwisted nematic LC cell with a twist angle higher than 140° is not an advantage for the optimization of the instrument.

Second, the maximum birefringence is analyzed. Note that by changing the maximum birefringence value, we are simulating different thickness of the TN-LC cell [20]. The EWV of the projection SOPs curve, using the specific values of TN-LC birefringence, are calculated. Figure 5 shows the evolution of the QI when the maximum birefringence increases. Note that the EWV is stabilized after 250° of maximum birefringence, approximately. Therefore, it is not necessary to work with higher birefringences (more than 250°). Moreover, working with thicker TN-LC cell leads to a slower response time.

We remark that the EWV values achieved in Figs. 4 and 5 are not comparable with those shown in Table 1, because the first ones correspond to characteristic curves (using 46 projection SOPs) and the others provided in Table 1 are for a set of 4 projection SOPs.

5. Conclusions

In summary, we present the optimization of six different polarimeters composed of a single TN-LC device. The advantage of using a single LC device is its simplicity and reduced cost compared with the standard polarimeters based on two LCDs. By modifying some parameters such as the optical path, the incidence angle or the projection polarization states, a significant improvement in the minimization of noise propagation is achieved. The optimized polarimeters were experimentally implemented, achieving excellent results for accuracy and repeatability. Experimental tests were developed in order to prove their correct performance for monochromatic and LED illumination. In particular, experimental measurements verify that the instrument is suitable to measure partially and fully polarized light. Finally, we have simulated polarimeters based on a TN-LC device with different values of maximum birefringence and twist angle. We have deduced that the most suitable TN-LC cell has a twist angle from 40° to 140° and a maximum value of birefringence around 250°.

Therefore, this work proves that dynamic Stokes polarimeters with very low error propagation values can be performed by using a single TN-LC device.

We acknowledge financial support from the Spanish Ministerio de Ciencia e Innovación (FIS2009-13955-C02-01) and the Generalitat de Catalunya (2011FI_B2 00140). C. Iemmi acknowledges the support from Universidad de Buenos Aires and the Consejo Nacional de Investigaciones Científicas y Técnicas (Argentina).

References

1. K. M. Twietmeyer, R. A. Chipman, Ann E. Elsner, Y. Zhao, and D. VanNasdale, "Mueller matrix retinal imager with optimized polarization conditions," Opt. Express **16**, 21339–21354 (2008).
2. M. Anastasiadou, A. De Martino, D. Clement, F. Liège, B. Laude-Boulesteix, N. Quang, J. Dreyfuss, B. Huynh, A. Nazac, L. Schwartz, and H. Cohen, "Polarimetric imaging for the diagnosis of cervical cancer," Phys. Status Solidi C **5**, 1423–1426 (2008).
3. A. Márquez, I. Moreno, C. Iemmi, A. Lizana, J. Campos, and M. J. Yzuel, "Mueller–Stokes characterization and optimization of a liquid crystal on silicon display showing depolarization," Opt. Express **16**, 1669–1685 (2008).
4. P. Y. Gerligand, M. Smith, and R. Chipman, "Polarimetric images of a cone," Opt. Express **4**, 420–430 (1999).
5. A. Peinado, A. Lizana, J. Vidal, C. Iemmi, and J. Campos, "Optimization and performance criteria of a Stokes polarimeter based on two variable retarders," Opt. Express **18**, 9815–9830 (2010).
6. J. M. Bueno, "Polarimetry using liquid-crystal variable retarders: theory and calibration," J. Opt. A **2**, 216–222 (2000).
7. A. De Martino, Y. K. Kim, E. Garcia-Caurel, B. Laude, and B. Drévillon, "Optimized Mueller polarimeter with liquid crystals," Opt. Lett. **28**, 616–618 (2003).
8. A. M. Gandorfer, "Ferroelectric retarders as an alternative to piezoelastic modulators for use in solar Stokes vector polarimetry," Opt. Eng. **38**, 1402–1408 (1999).

9. E. Garcia-Caurel, A. De Martino, and B. Drévillon, "Spectroscopic Mueller polarimeter based on liquid crystal devices," Thin Solid Films **455–456**, 120–123 (2004).
10. L. Gendre, A. Foulonneau, and L. Bigué, "Imaging linear polarimetry using a single ferroelectric liquid crystal modulator," Appl. Opt. **49**, 4687–4699 (2010).
11. L. B. Wolff and A. G. Andreou, "Polarization camera sensors," Image Vis. Comp. **13**, 497–510 (1995).
12. S. L. Blakeney, S. E. Day, and J. N. Stewart, "Determination of unknown input polarisation using a twisted nematic liquid crystal display with fixed components," Opt. Commun. **214**, 1–8 (2002).
13. D. Goldstein, *Polarized Light* (Marcel Dekker, 2003).
14. A. Lizana, N. Martín, M. Estapé, E. Fernández, I. Moreno, A. Márquez, C. Iemmi, J. Campos, and M. J. Yzuel, "Influence of the incident angle in the performance of liquid crystal on silicon displays," Opt. Express **17**, 8491–8505 (2009).
15. D. S. Sabatke, M. R. Descour, E. L. Dereniak, W. C. Sweatt, S. A. Kemme, and G. S. Phipps, "Optimization of retardance for a complete Stokes polarimeter," Opt. Lett. **25**, 802–804 (2000).
16. S. Huard, *Polarisation de la Lumière* (Masson, 1993).
17. J. A. Davis, I. Moreno, and P. Tsai, "Polarization eigenstates for twisted-nematic liquid-crystal displays," Appl. Opt. **37**, 937–945 (1998).
18. S. Stallinga, "Equivalent retarder approach to reflective liquid crystal displays," J. Appl. Phys. **86**, 4756–4766 (1999).
19. C. Soutar and K. Lu, "Determination of the physical properties of an arbitrary twisted-nematic liquid crystal cell," Opt. Eng. **33**, 2704–2712 (1994).
20. K. Lu and B. E. A. Saleh, "Theory and design of the liquid crystal TV as an optical spatial phase modulator," Opt. Eng. **29**, 1107–1113 (1990).